IRIS AperTO

UNIVERSITÀ DEGLI STUDI DI TORINO

AperTO - Archivio Istituzionale Open Access dell'Università di Torino

Methoxy-Substituted Copper Complexes as possible Redox Mediators in Dye-Sensitized Solar Cells

This is the author's manuscript

Original Citation:

Availability:

This version is available http://hdl.handle.net/2318/1801005 since 2021-09-13T12:06:22Z

Published version:

DOI:10.1039/d1nj02577e

Terms of use:

Open Access

Anyone can freely access the full text of works made available as "Open Access". Works made available under a Creative Commons license can be used according to the terms and conditions of said license. Use of all other works requires consent of the right holder (author or publisher) if not exempted from copyright protection by the applicable law.

(Article begins on next page)

26 December 2024

IRIS AperTO

UNIVERSITÀ DEGLI STUDI DI TORINO

This is the author's final version of the contribution published as:

Marco Giordano, Giorgio Volpi, Matteo Bonomo, Paolo Mariani, Claudio Garino, Guido Viscardi.

Methoxy-substituted copper complexes as possible redox mediators in dye-sensitized solar cells

New Journal of Chemistry, 2021, 45, 15303.

DOI: 10.1039/d1nj02577e

The publisher's version is available at:
https://pubs.rsc.org/en/content/articlelanding/2021/nj/d1nj02577e

When citing, please refer to the published version.

Link to this full text:
http://hdl.handle.net/2318/1801005

This full text was downloaded from iris-Aperto: https://iris.unito.it/

iris-AperTO

University of Turin's Institutional Research Information System and Open Access Institutional Repository

Methoxy-Substituted Copper Complexes as possible Redox Mediators in Dye-Sensitized Solar Cells

M. Giordano[a], G. Volpi[a], M. Bonomo[a], P. Mariani[b], C. Garino[a]*, G. Viscardi[a]

[a]*Department of Chemistry, NIS Interdepartmental Centre and INSTM Reference Centre, University of Turin, 10125 Turin, Italy*
[b]*CHOSE and Dept. of Electronic Engineering, University of Rome "Tor Vergata", via del Politecnico 00133 Rome, Italy*
* corresponding author claudio.garino@unito.it

Abstract

Three aromatic diimine ligands and the corresponding homoleptic copper(I) and copper(II) complexes have been synthetized and characterized. The copper(II) derivatives are stabilized by an ancillary chlorido ligand. The nature of the chelating ligand seriously impacts on the photophysical and electrochemical properties of the complexes. The substitution of the pendant methyl groups with methoxy influences the coordination geometry of the complex, resulting in an intramolecular dynamic equilibrium between different coordination modes (i.e. nitrogen and oxygen binding), proved by variable-temperature ^{1}H-NMR measurements. As a proof of concept, the most promising complexes were employed as redox mediators in semi-transparent Dye-Sensitized Solar Cells. Once implemented in device, the nature of the ligand plays a crucial role: the methoxy-substituted derivatives occur in severe ligand exchange with *tert*-butylpyridine, resulting in a unexpectedly high open circuit voltage.

1. Introduction

In the last decades, transition-metal complexes have been deeply studied and employed for several applications such as: photoredox catalysis[1,2], bioimaging[3], water splitting[4], lightening[5,6] and solar conversion (Dye-Sensitized Solar Cells)[7-10]. However, most of them are based on rare and very expensive metals, resulting in significant limitation to achieve the development of economic and environmentally sustainable applications. A springboard to overcome these limitations may be the use of copper, thanks to its abundance, cheapness, low toxicity and great recycle value. The environmentally friendly properties of copper make it appealing for a wide type of applications among which, Dye-Sensitized Solar Cells (DSSCs) represent an interesting example[11,12]. In this context, metal complexes have been studied both as photosensitizers and as redox couples to overcome the sustainability limitations of ruthenium(II)-based photosensitizers and cobalt-based redox couples, respectively[9,13-15]. Metal-based complexes allow to finely tune the open circuit potential of the resulting devices by modification of both metal centre and ligands[8-10]. Among the former, cobalt and copper are the most exploited metal centre assuring relatively deep redox potential values (even lower than 0.7 V vs NHE) and, in turns, open circuit voltage (V_{OC}) values higher than 1 V[9]. The high V_{OC} coupled with a decent current density allows to break the wall of 10% in efficiency. Furthermore, copper complexes are especially attractive due to the possibility to develop redox couples both as liquid electrolytes or as solid state hole transport materials (HTMs)[16,17] exploitable both in liquid and (quasi)-solid state DSSCs[9,18-21]. They are particularly interesting as efficient redox mediator because of their characteristic fast electron self-exchange. This property may reduce charge transport limitations, and thus the electrolyte may allow higher overall conversion efficiencies[22,23]. Unfortunately, some drawbacks are still present when implemented in complete device: indeed, compared to cobalt-based redox couples, copper complexes present (i) larger visible absorption that could cause a parasitic light absorption and (ii) slower regeneration kinetic due to the marked difference in the coordination geometry of the reduced and the oxidized species that could lead to energy losses during the redox process. More in detail, copper(I) complexes are characterized by a d^{10} electronic configuration in tetrahedral geometry, while copper(II) show a d^9 configuration widening the coordination sphere[24-26]. To limit the impact of complexes reorganization, a valuable approach could be the design of tailored ligands. Aiming at a different application, Fukuzumi and co-workers reported that sterically hindered substituents on the copper coordination sites of copper-blue proteins induce both copper(I) and copper(II) to rearrange into a distorted tetragonal geometry, lowering the reorganization energy and, as consequence, improving the process kinetic[27].

The present study is focused on the synthesis and characterization of six homoleptic copper complexes, depicted in Fig. 1. In complexes **1**-**3a** the copper shows oxidation state +1, while for the corresponding complexes **1**-**3b** the oxidation state of copper is +2. The compounds can be combined in three redox couples, characterized by a relatively weak absorption in the visible range, good chemical stability and, more important, high redox potential leading to promising V_{OC} once implemented in complete devices. The two bipyridine ligands were chosen getting inspired by literature[28]. The bipyridine was decorated by methyl groups (complexes **1a**, **1b**, state-of-art redox mediator) while replacing methyl with methoxy substituents provided the second ligand (complexes **2a**, **2b**), chosen to evaluate the effect of the electron donating group as well as the possible stabilization effect induced by the proximal oxygen atom. Finally, a third ligand based on the electron-rich imidazo[1,5-*a*]pyridine skeleton was selected to obtain complexes **3a** and **3b**.

Recently, this heterocyclic moiety has been successfully employed in optoelectronic devices as a very promising alternative to the widely investigated bipyridines[29-32]. As proof of concept, **1a**/**1b** chosen as

reference, and **2a**/**2b** have been tested as redox couples in DSSCs sensitized with MK2 dye (depicted in Fig. 2), leading to promising results.

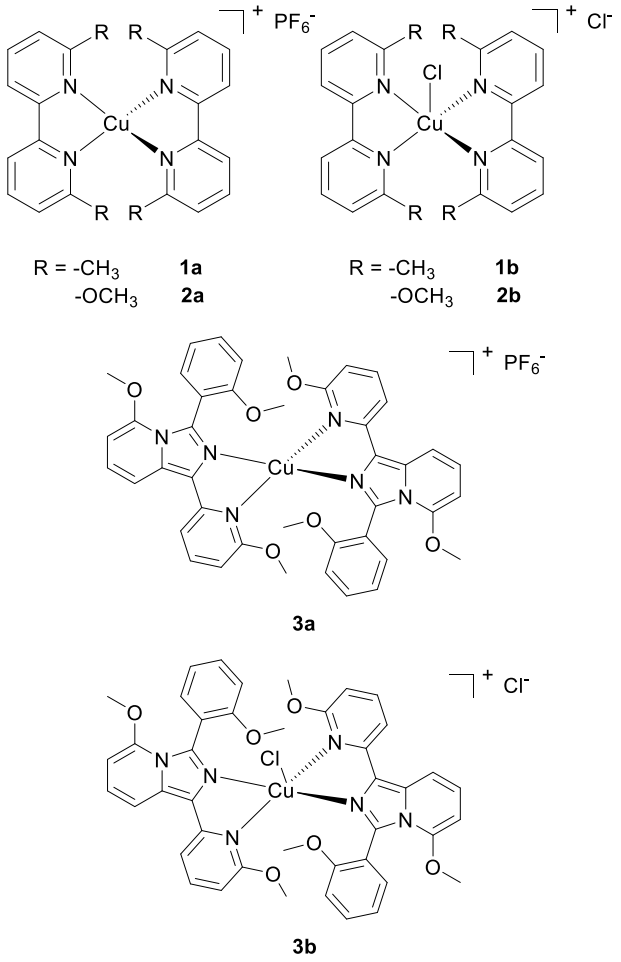

Fig. 1. Molecular structures of copper(I) complexes (**1**-**3a**) and copper(II) complexes (**1**-**3b**).

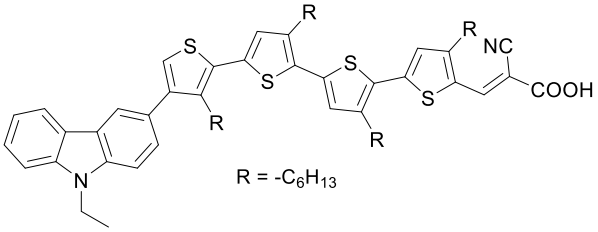

Fig. 2. Molecular structure of MK2.

2. Experimental section

2.1 Materials and methods

All solvents and chemicals were purchase from Merck Life Science and Alfa Aesar and were used as received without further purification. Synthesis of bipyridine ligands was done in a Biotage Initiator Plus microwave oven. ^{1}H- and ^{13}C-NMR spectra were recorded on a JEOL ECP 400 FT-NMR spectrometer (^{1}H-NMR operating frequency 400 MHz). Chemical shifts are reported relative to TMS (δ = 0) and referenced against solvent residual peaks. The following abbreviations are used: s (singlet), d (doublet), t (triplet), dd (doublet of doublets), m (multiplet), br (broad). Mass spectra were recorded on a Thermo Scientific LCQ Advantage Max mass spectrometer. Elemental composition was determined using a Thermo FlashEA 1112 CHNS–O analyser, two replicas were performed, and values were presented as % mass mean value. UV-Vis

absorption data were acquired on a Shimidazu PharmaSpec UV-1700 spectrophotometer. FT-IR absorption spectra were performed using Perkin Elmer UATR Two spectrometer by ATR technique. Cyclic voltammetry measurements were performed using a Bio-Logic SP150 potentiostat, with a three-electrode configuration: Ag/AgCl/saturated LiCl (ethanol) reference electrode, glassy carbon working electrode and platinum wire counter electrode. All copper complexes were analysed under argon at 200 mV/s scan rate. Copper complexes were dissolved in dichloromethane (or acetonitrile), with tetrabutylammonium hexafluorophosphate (0.1 M) as supporting electrolyte. Redox potentials were primarily referenced versus the ferrocene/ferrocenium redox couple (measured $E_{1/2}(0/+1)$ = 0.463 V in CH_2Cl_2 vs. Ag/AgCl) employed as internal standard.

2.2 Synthesis of ligands

The synthesis of bipyridine ligands was carried out according to published procedures[33,34], with standard heating and in microwave reactor. Quantitative yields with significantly reduction of solvent amount and reaction times were obtained in the present study operating in a sealed microwave tube reactor. A mixture of nickel chloride hexahydrate (3.05 mmol, 1 eq.), triphenylphosphine (12.2 mmol, 4 eq.) and zinc powder (9.15 mmol, 3 eq.) in 15 mL of DMF was sealed in a microwave tube reactor and stirred under nitrogen for one hour. After that, the halopyridine (3.05 mmol, 1 eq.) was added and the reaction carried out at 120 °C for 45 minutes. Then, the reaction was cooled at room temperature, quenched by 5 mL of NH_3 25% and the resulting mixture was extracted three times with CH_2Cl_2. The organic phase was separated, dried over Na_2SO_4 and evaporated under vacuum.

6,6'-dimethyl-2,2'-bipyridine (*dMe-bpy*). The crude was purified by flash chromatography (98:2 dichloromethane/methanol). The product was isolated as a white solid (0.27 g, 97%). TLC R_f (DCM): 0.12. FT-IR (ν_{max}/cm^{-1}): 3064, 2924, 1573, 1437, 1080, 781. ^{1}H-NMR (400 MHz, $CDCl_3$) δ 8.16 (d, 2H, *J* = 7.8 Hz, CH), 7.66 (t, 2H, *J* = 7.8 Hz, CH), 7.12 (d, 2H, *J* = 7.4 Hz, CH), 2.59 (s, 6H, CH_3). ^{13}C-NMR (100 MHz, $CDCl_3$) δ 157.9, 155.8, 137.3, 123.3, 118.4, 24.7. MS (ESI+, CH_3OH): *m/z* 185.19 (M+H$^+$, 100%).

6,6'-dimethoxy-2,2'-bipyridine (*dMeO-bpy*). The crude was purified by flash chromatography (100% Petroleum ether). The product was isolated as a white solid. (0.32 g, 98%). TLC R_f (DCM): 0.60. FT-IR (ν_{max}/cm^{-1}): 2950, 1574, 1460, 1399, 1296, 1020, 789. ^{1}H-NMR (400 MHz, $CDCl_3$) δ 8.02 (dd, 2H, *J* = 7.6 Hz, *J* = 0.8 Hz, CH), 7.69 (t, 2H, *J* = 7.9 Hz, CH), 6.76 (dd, 2H, *J* = 8 Hz, *J* = 0.8 Hz, CH), 4.04 (s, 6H, CH_3). ^{13}C-NMR (100 MHz, $CDCl_3$) δ 163.5, 153.5, 139.3, 113.7, 111.0, 53.3. MS (ESI+, CH_3OH): *m/z* 217.13 (M+H$^+$, 100%).

5-methoxy-3-(2-methoxyphenyl)-1-(6-methoxypyridin-2-yl)H-imidazo[1,5-a]pyridine (*impy*). The ligand was prepared with a slight modification of a previously reported procedure[29,35]. A mixture consisting of bis(6-methoxypyridin-2-yl)methanone (2.00 mmol, 488 mg), 2-methoxybenzaldehyde (2.00 mmol, 272 mg), and ammonium acetate (10.00 mmol) in 25 mL of glacial acetic acid was stirred at 120 °C. After 12 h, the reaction mixture was cooled to room temperature and the acetic acid was removed by evaporation under vacuum. The solid was dissolved in an aqueous solution of Na_2CO_3 and the mixture extracted with CH_2Cl_2. The organic layer was separated and the solvent evaporated under vacuum. The formed solid was washed several times with diethyl ether and dried under vacuum obtaining a yellow powder (0.51 g, 70%). TLC R_f (DCM/MeOH 98:2): 0.45. FT-IR (ν_{max}/cm^{-1}): 2964, 1757, 1532, 1243, 1031, 805, 739. ^{1}H-NMR (400 MHz, acetone-d6) δ 8.37 (d, 1H, *J* = 8 Hz, CH), 7.57 (m, 2H, Ar-H), 7.36-7.45 (m, 2H, Ar-H), 6.99-7.07 (m, 3H, Ar-H), 6.55 (d, 1H, *J* = 6.5 Hz, CH), 6.07 (d, 1H, *J* = 6.5, CH), 4.06 (s, 3H, CH_3), 3.70 (s, 3H, CH_3), 3.68 (s, 3H, CH_3). ^{13}C-NMR (100 MHz, acetone-d6) δ 138.7, 131.8, 130.8, 124.0, 120.3, 113.6, 112.7, 110.8, 109.8, 89.7, 66.1, 57.7, 56.7, 55.7, 55.0, 53.7, 18.9, 15.6. MS (ESI+, CH_3OH): *m/z* 362.18 (M+H$^+$, 100%).

2.3 Synthesis of copper(I) complexes

The synthesis of copper(I) complexes were performed according to published general procedures[36,37]. A mixture of tetrakis(acetonitrile)copper(I) hexafluorophosphate (1 eq.) and of the corresponding ligand (2.2 eq.) in 10 mL of dichloromethane was stirred under nitrogen at room temperature for 3 hours. The reaction mixture was concentrated and the raw material purified by repeated washings with a diethyl ether/petroleum ether solution (1:1).

[Cu(dMe-bpy)$_2$]PF$_6$ (**1a**). The product was isolated as a bright red solid (0.27 g, 85%). FT-IR (ν_{max}/cm^{-1}): 1599, 1462, 833, 786. ^{1}H-NMR (400 MHz, $CDCl_3$) δ 8.20 (d, 2H, *J* = 8 Hz, CH), 8.00 (t, 2H, *J* = 7 Hz, CH), 7.44 (d, 2H, *J* = 6 Hz, CH), 2.23 (s, 6H, CH_3). ^{13}C-NMR (100 MHz, $CDCl_3$) δ 157.3, 151.7, 138.6, 126.0, 119.7, 25.3. Elemental analysis Found: C, 49.8; H, 4.3; N, 9.4 Calc. for $CuC_{24}H_{24}N_4PF_6$: C, 50.0; H, 4.2; N 9.7%. MS (ESI+, CH_3OH): *m/z* 431.48 (M^+, 100%), 246.13 (13).

[Cu(dMeO-bpy)$_2$]PF$_6$ (**2a**). The product was isolated as a dark red-brown solid (0.23 g, 79%). FT-IR (ν_{max}/cm^{-1}): 1571, 1474, 1260, 1031, 833, 790. ^{1}H-NMR (400 MHz, $CDCl_3$) δ 7.88 (br, 4H, Ar-H), 6.87 (br, 2H, Ar-H), 3.96 (br, 6H, CH_3). ^{13}C-NMR (100 MHz, $CDCl_3$) δ 163.8, 151.5, 141.9, 115.0, 108.8, 53.8. Elemental analysis Found: C, 44.7; H, 3.95; N, 8.5 Calc. for $CuC_{24}H_{24}N_4O_4PF_6$: C, 45.0; H, 3.8; N, 8.7%. MS (ESI+, CH_3OH): *m/z* 495.11 (M^+, 100%), 279.07 (45), 296.66 (17).

[Cu(impy)$_2$]PF$_6$ (**3a**). The product was isolated as a bright red solid (0.19 g, 76%). FT-IR (ν_{max}/cm^{-1}): 2947, 1531, 1278, 1009, 830. ^{1}H-NMR (400 MHz, $CDCl_3$) δ 7.69 (br, Ar-H), 7.54 (br, Ar-H), 7.13 (br, Ar-H), 6.69 (br, Ar-H), 6.41 (br, Ar-H), 6.15 (br, Ar-H), 3.74 (br, CH_3), 3.59 (br, CH_3). Elemental analysis Found: C, 54.0; H, 4.2; N, 8.7 Calc. for $CuC_{42}H_{38}N_6O_6PF_6$: C, 54.2; H, 4.1; N, 9.0%. MS (ESI+, CH_3OH): *m/z* 785.21 (M^+, 100%).

2.4 Synthesis of copper(II) complexes

The synthesis of copper(II) complexes were performed according to published procedures[38]. A mixture of anhydrous $CuCl_2$ (1 eq.) and ligand (2.2 eq.) in 10 mL of dichloromethane was stirred under air flux at room temperature for 3 hours. The reaction mixture was concentrated and the raw material purified by repeated washings with a diethyl ether/petroleum ether solution (1:1); the reaction was monitored by TLC (98:2 dichloromethane/methanol) until the ligand disappears. Despite the paramagnetic nature of copper(II) complexes, it was possible to acquire the ^{1}H-NMR spectra for the two bipyridine-based complexes, even though the resonances are very broad.

[Cu(dMe-bpy)$_2$Cl]Cl (**1b**). The product was isolated as a green solid (0.06 g, 22%). FT-IR (ν_{max}/cm^{-1}): 3382, 1600, 1444, 1001, 796. ^{1}H-NMR (400 MHz, $CDCl_3$) δ 8.83 (br, 2H, Ar-H), 8.10 (br, 2H, Ar-H), 7.48 (br, 2H, Ar-H), 2.99 (br, 6H, CH_3). Elemental analysis Found: C, 57.1; H, 5.0; N, 10.85 Calc. for $CuC_{24}H_{24}N_4Cl_2$: C, 57.3; H, 4.8; N, 11.1%. MS (ESI+, CH_3OH): *m/z* 466.10 (M^+, 100%), 281.91 (38).

[Cu(dMeO-bpy)$_2$Cl]Cl (**2b**). The product was isolated as a bright green solid (0.20 g, 78%). FT-IR (ν_{max}/cm^{-1}): 3457, 1573, 1477, 1267, 1145, 1028, 792. ^{1}H-NMR (400 MHz, $CDCl_3$) δ 8.22 (br, 4H, Ar-H), 7.05 (br, 2H, Ar-H), 4.17 (br, 6H, CH_3). Elemental analysis Found: C, 50.5; H, 4.5; N, 9.65 Calc. for $CuC_{24}H_{24}N_4O_4Cl_2$: C, 50.85; H, 4.3; N, 9.9%. MS (ESI+, CH_3OH): *m/z* 895.04 ([Cu_2(*dMeO-bpy*)$_3Cl_2$(CH_3OH)OH]$^+$, 100%), 494.96 (17), 313.88 (13).

[Cu(impy)$_2$Cl]Cl (**3b**). The product was isolated as a dark green solid (0.15 g, 63%). FT-IR (ν_{max}/cm^{-1}): 2942, 1639, 1534, 1486, 1279, 999, 789. Elemental analysis Found: C, 58.6; H, 4.65; N, 9.7 Calc. for $CuC_{42}H_{38}N_6O_6Cl_2$: C, 58.85; H, 4.5; N, 9.8%. MS (ESI+, CH_3OH): *m/z* 819.68 (M^+, 100%), 460.88 (10).

2.5 Solar device fabrication

Glass FTO (Flourine doped Tin Oxide) covered substrate is provided from "NSG-Pilkington" with a sheet resistance of 7 Ω sq^{-1}. It was cut in 15x20 cm^2 size and was cleaned using "Hellmanex" cleaning solution diluted with water in a 2:98 v/v ratio, acetone and 2-propanol in an ultrasonic bath (10 minutes each). At the end, substrates are rinsed in 2-propanol and quickly dried with a strong air flow. Just after the cleaning, an UV-O_3 treatment is performed by PSD Pro Series Digital UV Ozone System from "Novascan" in order to remove the organic contaminations[39]. Photo-electrode (PE) was fabricated in two steps. The first one, is obtained depositing a compact TiO_2 layer. Just after the UV-O_3 treatment, the FTO/glass substrate is transferred to a hot plate and warmed up to 460 °C (within 35 minutes). The substrate is left for 10 min at 460 °C before depositing the compact TiO_2 layer by manual spray pyrolysis. The sprayed solution is composed by 0.5 mL of acetylacetone (from Merck) and 0.75 mL of titanium(IV) diisopropoxide bis(acetylacetonate) from Sigma-Aldrich), in 11.25 mL of ethanol (EtOH), which is enough to cover the entire substrate. The nozzle of the airbrush is about 40 cm far from the FTO surface. The gas carrier is air at a pressure of 1.6 bar. The nozzle forms an angle of about 45°C respect to the plane of the substrate and it was moved according to a serpentine path, for 12 cycles (one every 10 seconds) in order to reach around 50 nm in thickness (measured via profilometry (Deektat Veeco 150)). Then, the substrates are left for 15 minutes at 460 °C before cooling them down slowly to room temperature. The second step involved the realization of PE is the deposition of a mesoporous layer of TiO_2 by screen printing technique over the compact TiO_2 layer. We printed a mesoporous layer of TiO_2 paste 18 N-RT (from Great Cell Solar), based on 20 nm TiO_2 particles, onto the substrate by means of a screen with mesh 48T (i.e., 48 threads in the polyester screen/cm). The printing was performed in double squeegee mode. Just after the printing, the mesoporous layer was left at rest for 10 minutes to allow its surface relaxing in order to promote its levelling. Then the layer is dried at 120 °C for 20 min in an oven, a Lenton WHT6/60 (Hope Valley, U.K.). Then PE is then sintered at 525 °C for 30 min in the same oven, in order to decompose the organic binders in the paste and to promote electromechanical connection between the TiO_2 nanoparticles[40]. Its final thickness was around 5.5 µm and it is measured via profilometry (Deektat Veeco 150). To perform sensibilization processes, the still warm electrodes were immersed in an absolute ethanol solution of MK2 dye from Dyesol (i.e. 0.3 mM) for 4 hours at room temperature. After sensitization, they were washed with ethanol to remove the excess of not chemisorbed dye. Then, they were assembled in a sandwich configuration with a Pt-based counter-electrode, obtained following well established receipts[41]. A Bynel® thermoplastic film was used as both spacer and sealant. For each electrolytes four different cells were tested. Iodine-based electrolyte was prepared mixing 0.05 M of iodine, 0.1 M of lithium iodide, 0.5 M 1-methyl-3-propyl-imidazolium iodide (PMII) and 0.5 M 4-tert-butylpyridine (TBP). Copper-containing electrolytes were prepared in two different ways: (i) by dissolving the desired Cu(I) complex (0.25 M) in a suitable amount of acetonitrile/valeronitrile (7:3) with $LiClO_4$ 0.12 M; due to the undesired synthesis of pentacoordinated species, the Cu(II) tetracoordinated counterpart was prepared inside the cell by photo-oxidation; (ii) by adjusting the Cu(I)/Cu(II) ratio by addition of the proper amount of a $NOBF_4$ solution (0.3 M in acetonitrile). In both cases, suitable volumes of 4-*tert*-butylpyridine were finally added to reach 0.5 M concentration in the electrolyte solution; lastly, the solution was injected in the cell by back-vacuum filling technique using a hole in the spacer. After the injection of the electrolyte, the hole was sealed with a commercial bicomponent resin. Photoelectrochemical performances were tested using a solar simulator Solar Test 1200 KHS at 1000 W/m^{-2} (artificial solar spectrum AM 1.5G).

3. Results and discussion

The synthetic effort in this work concerns the production of new homoleptic Cu(I) complexes and of their Cu(II) analogues. The study and comparison of these compounds, in which the metal exhibits different

oxidation states, are critical for understanding the activity of the redox mediator in DSSC devices. The studied products were synthesised according to published procedures[28,36,42,43]. For the Cu(I) derivatives, we reacted the proper ligand with the tetrakis(acetonitrile)copper(I) hexafluorophosphate precursor, under inert atmosphere to avoid copper oxidation. The Cu(II) analogues were synthesized starting from anhydrous $CuCl_2$ in dichloromethane under air flow, to avoid copper autoreduction[38]. The ancillary Cl^- ligand is fundamental to stabilise the Cu(II) oxidation state, promoting the pentacoordinate geometry and avoiding the possible autoreduction to tetrahedral Cu(I). The Cu(I) complexes were collected as red hexafluorophosphate solid salts while the Cu(II) complexes as green chloride powders. All the complexes were characterized by mass spectrometry, elemental analysis, cyclic voltammetry, UV-Vis and NMR spectroscopy.

The mass spectra of all the obtained complexes are consistent with the proposed structures. In the ESI+ spectra of Cu(I) compounds, the main peak is due to the singly charged molecular cation (**1a** *m/z* = 431.48, **2a** *m/z* = 495.11, **3a** *m/z* = 785.21). The same happens for the Cu(II) derivatives (**1b** *m/z* = 466.10, **3b** *m/z* = 819.68). For **2b**, the molecular cation was not detected, instead a peak at *m/z* = 895.04 can be observed. This can be assigned to a dimeric form $[Cu_2(dMeO\text{-}bpy)_3Cl_2(CH_3OH)OH]^+$ which is a gas phase ion formed under ESI conditions. Characteristic isotope patterns for copper- and chlorine-containing ions are clearly seen, confirming the elemental composition of the ions observed.

The ^{1}H-NMR spectrum of **1a** is characterized by well-resolved signals and shows no broadening, in agreement with previously reported data. On the other hand, the ^{1}H-NMR spectra of complexes **2a** and **3a** are characterized by broad peaks lacking any multiplicity information. The broadening is not due to paramagnetic Cu(II) impurities, whose absence is confirmed by other experimental evidence (no signals ascribable to Cu(II) compounds in ESI-MS and in cyclic voltammetry measurements). To clarify the origin of the peak broadening, we performed a series of variable-temperature ^{1}H-NMR measurements in acetone-d6, down to 203 K. As shown in Fig. 3a, lowering the temperature results in a progressive narrowing of the resonances for **2a**, until the complete recover of the spectral resolution at 203 K. At this temperature, the spectrum consists of three narrow signals, a doublet and a triplet in the aromatic portion and a singlet for the methoxy substituents in the aliphatic region. The proton NMR of **3a** is more intricate (depicted in Fig. 3b); at room temperature the spectrum is characterized by the presence of multiple sets of broad peaks. At low temperature, the signal broadening progressively decreases unveiling the signal multiplicity. At 203 K, the spectrum of **3a** clearly displays three sets of narrow resonances. Analysis of the integration revealed a 2:1:1 ratio, particularly evident in the aliphatic region.

The abovementioned data suggest, for **2a** and **3a**, the presence of an intramolecular dynamic equilibrium between different coordination modes, involving the coordination through the oxygen atom of the methoxy substituents, in competition with the pyridine nitrogen atoms. These coordination patterns have been previously observed in Cu complexes containing N,O ligands[44]. At low temperature, the signals resolution and multiplicity are recovered due to the slower kinetic of such coordination equilibrium. Finally, it is worth noting that the ^{1}H-NMR spectra do not evidence the classical pattern of the free ligand, excluding the possibility of the ligand dissociation. Due to the paramagnetic nature and to the low solubility of the Cu(II) complexes, it was not possible to perform a complete NMR characterization for **1b**–**3b**. We were however able to acquire ^{1}H-NMR spectra for **1b** and **2b**; although the signals are very broad, the integration ratio are respected and the signals are shifted to higher frequencies, in agreement with the higher oxidation state of the metal centre.

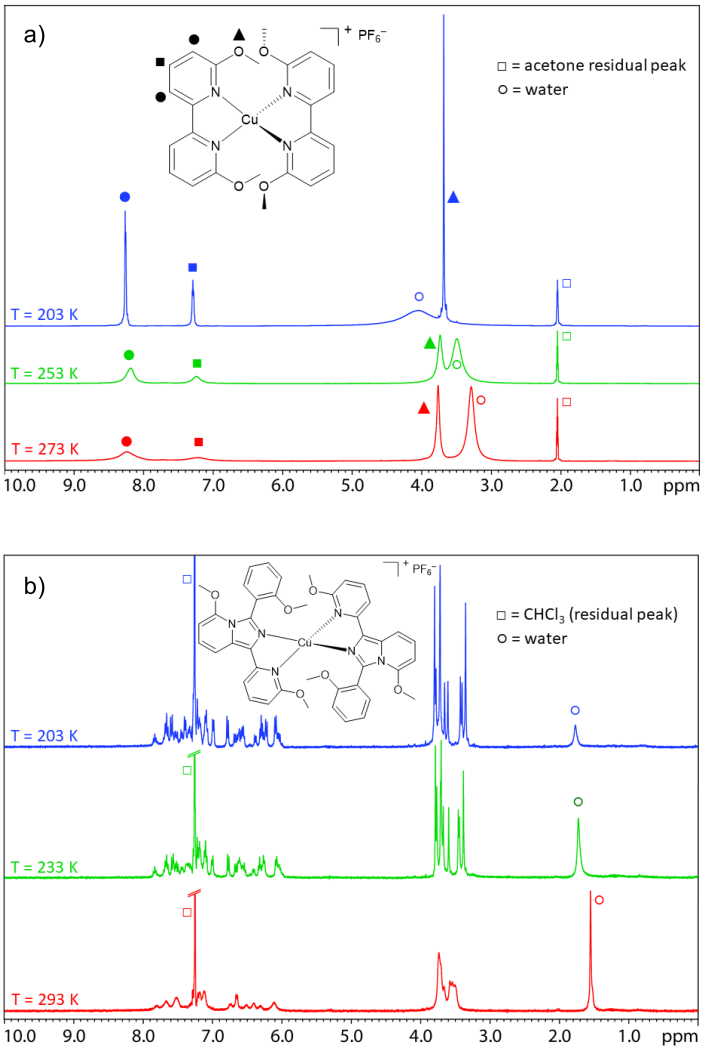

Fig. 3. Variable-temperature ^{1}H-NMR spectra of (a) complex **2a** in acetone-d6 and (b) complex **3a** in $CDCl_3$.

3.1 Optical spectroscopy

A low molar extinction coefficient in the visible region is a fundamental prerequisite for a suitable redox mediator in DSSCs, to avoid the competition with the dye in visible light absorption. The absorption spectra of both Cu(I) and Cu(II) complexes are gathered in dichloromethane solution (Fig. 4). The complexes bearing the bipyridine ligands (*dMe-bpy* and *dMeO-bpy*) display the principal absorption band below 350 nm, typical of the bipyridine moiety. On the other hand, for **3a** and **3b** the main absorption is centred at 380 nm, as expected for compounds containing the imidazo[1,5-*a*]pyridine moiety[45-48]. The copper(I) complexes show a characteristic absorption in the visible region around 450 nm, attributed to a metal-to-ligand charge transfer (MLCT) (Fig. 4a). By comparing these signals, it is possible to observe the effect of the methoxy group on the shape of the MLCT signal. The complex **2a** shows a broad MLCT band and a lower molar extinction coefficient if compared to **1a**, see Tab. 1. Otherwise, **3a** does not show a maximum but the MLCT signal appears as a broad shoulder between 450-550 nm. All the three Cu(I) complexes display very low molar extinction coefficients. The copper(II) complexes display the same absorption profile of the corresponding copper(I) compounds, in the UV region. Moreover, in the visible range, the copper(II) derivatives show a characteristic broad absorption at 650-750 nm, due to the *d-d* electronic transition (Fig. 4b, inset). These bands are characterized by a very low molar extinction coefficient (< 2000 M^{-1} cm^{-1}).[43]

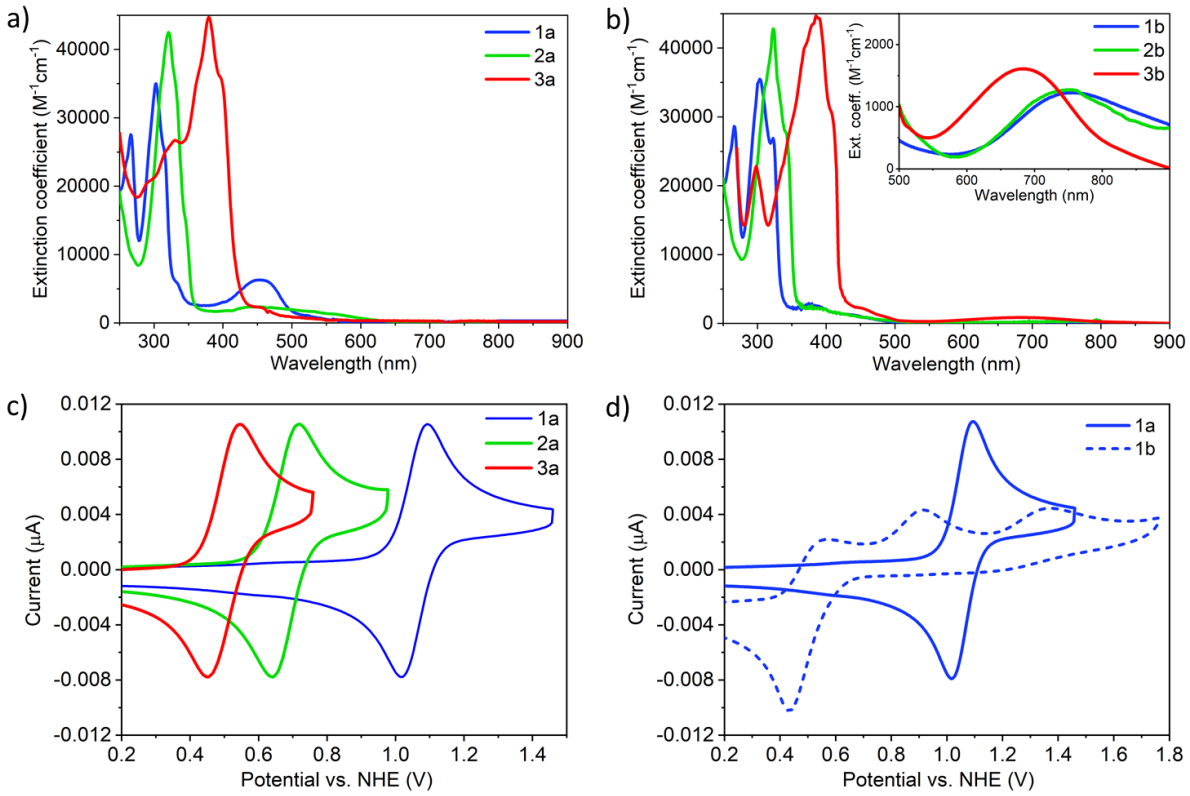

Fig. 4. UV-Vis absorption spectra of (a) Cu(I). (b) Cu(II) complexes in dichloromethane solution. (c) Cyclic voltammograms of Cu(I) complexes. (d) Cyclic voltammograms of **1a** and **1b**. Measurements have been performed in 0.1 M tetrabutylammonium hexafluorophosphate/dichloromethane. Scan rate 200 mV/s. Potentials are referenced to NHE.

Tab. 1 Electrochemical and optical data for **1**-**3a**.

	ε / M^{-1} cm^{-1} (wavelength / nm)	$E_{1/2}$ Cu(I)/Cu(II) / V vs. NHE
1a	6500 (454)	1.06[b]
2a	2350 (445)	0.68[b]
3a	2800 (455)[a]	0.50[b] 1.50[c]

ε: extinction coefficient, $E_{1/2}$: formal redox potential.
[a] Shoulder.
[b] Determined from the voltammogram of Cu(I) species only.
[c] Second oxidation attributed to the ligand.

3.2 Electrochemical data

The redox potentials of the investigated complexes are tabulated in Tab. 1. The copper(I) complexes **1a** and **2a** show a single oxidation due to a metal-centred process (Figure 4c). On the other hand, **3a** displays also a second signal at higher potential (1.50 V), due to the typical reversible oxidation process of the imidazo[1,5-*a*]pyridine ligand (not shown in figure 4c)[30,49,50]. The substitution on the bipyridine ligands has a direct influence on the redox potential of the complexes. The methoxy substituent groups provide a lower redox potential for **2a** respect to **1a**, due to its higher electron donor behaviour and its smaller steric hindrance compared to the methyl group; this behaviour is in good agreement with literature findings[42,51]. The comparison between the bipyridine-based complexes highlights that, if the steric hinderance of the substituent near the coordination site increases, the potential of Cu^{2+}/Cu^{+} transition raises. Indeed, during the oxidation process, the metal centre must convert from the typical tetrahedral structure of copper(I)

complexes to a distorted tetragonal geometry, typical of copper(II) complexes[24-26]. The complex **3a** shows a lower oxidation potential compared to the bipyridine-based complexes, suggesting a high capacity of the imidazo[1,5-*a*]pyridine ligands to provide electron density towards the metal centre. The electrochemical data of the copper(II) complexes provide important information about their structural and electronic properties. In agreement with literature findings[51], the copper(II) complexes display a more intricate redox behaviour, characterized by multiple oxidation steps[42]. In particular, the copper(II) complexes are characterized by multiple-wave voltammograms (Figure 4d, S3-S4); where the pentacoordinated structure containing the chlorine atom coordinated to the metal centre is subjected to structural changes, as reported in literature[36]. Cyclic voltammograms of **1a** and **2a** performed in acetonitrile show less reversible signals, due to a possible interaction with the solvent, during the oxidation process (**1a** E_{ox1} = 0.79 V E_{ox2} = 1.04 V, **2a** E_{ox1} = 0.76 V E_{ox2} = 1.19 V).

3.3 Dye Solar Cells tests

As a proof of concept, we decide to employ the most promising complex (i.e. **2a**) as liquid redox mediator in semi-transparent Dye-Sensitized Solar Cells. It is worth mentioning that the pentacoordinated species of Cu(II) complex could lead to quite complicated redox processes; therefore, **2b** was not directly dissolved in the electrolyte solution but it was obtained inside the cell starting from the copper(I) complex **2a**, following procedures previously reported in literature (see experimental section for further details)[51]. The first approach consists in the insertion of an electrolyte containing the sole Cu(I) complex in the device. Then, the cell is continuously illuminated in order to promote the light-driven oxidation into Cu(II). The photoelectrochemical performances were continuously recorded: initially, all the photovoltaic figure of merit gradually increased following on from the partial conversion of Cu(I) to Cu(II). After ten minutes, photoelectrochemical parameters stabilize obtaining a photoconversion efficiency up to 0.87%. Such a relatively low value is mainly due to an extremely low fill factor (FF) (i.e. 0.23) accounting for fast recombination reactions. Additionally, we can assume a relatively small Cu(I) → Cu(II) light-driven conversion. Some recent literature reports proved that when the complex is in its higher oxidation state (i.e. Cu(II)) it could incur in ligand exchange, being the pyridine ligand substituted by both (mainly) acetonitrile and 4-*tert*-butylpyridine (TBP), especially if the latter is present in a higher concentration with respect to the Cu(II) salt[52,53]. The presence of one or more TBP in the complex structure will cause a reduction in the diffusion coefficient of Cu(II) species and a slowdown in its regeneration kinetic at the counter-electrode. The occurrence of such ligand-exchange is also confirmed by the relatively high photovoltage recorded. As a matter of fact, considering the pure **2a**/**2b** couple, a photovoltage of maximum 800 mV could be expected, and this value will be also negatively affected by sizeable recombination reactions. Indeed, a V_{OC} of 856 mV was recorded. To further confirm this, we performed some ESI-MS analyses in which some characteristic peak of acetonitrile and/or TBP coordinated species could be evidenced (see Fig. S1-S2 and discussion therein). Moreover, also the CV of **2a** in acetonitrile shows a clear instability of the complex probably due to a partial ligand exchange caused by the solvent.

A different approach consists in the employment of $NOBF_4$ as oxidant. In this case, the addition of BF_4^- as counter-ion could partially prevent the ligand exchange due to the stabilization of the Cu(II) complex: indeed, some TBP and acetonitrile based derivatives could be still detected in ESI-MS, but their relative ratio with **2a** is lower than in the previous case. The oxidant was added in the electrolyte solution before the insertion in the device. The effect on the photoelectrochemical parameters is dramatic: the FF (0.63) and photoconversion efficiency (2.70%) are more than doubled. The photovoltage is about 60 mV lower accounting for a higher redox potential of the redox couple: in fact, $NOBF_4$ assures a higher Cu(I) → Cu(II) conversion. Therefore, $E_{Cu(I)/Cu(II)}$ shifted at lower potential, according to Nerst's equation. Simultaneously, a reduction in the occurrence of recombination reactions is evidenced by a higher FF.

Tab. 2 DSSCs performance with the different types of electrolyte.

Electrolyte	V_{OC} / mV	J_{SC} / mA cm^{-2}	*Fill Factor*	η / %
2a	856 ± 38	4.43 ± 0.22	0.23 ± 0.10	0.87 ± 0.18
2a + $NOBF_4$	804 ± 22	5.33 ± 0.58	0.63 ± 0.03	2.70 ± 0.12
2a + $NOBF_4$ w/o TBP	585 ± 18	3.71 ± 0.33	0.51 ± 0.02	1.11 ± 0.09
I^-/I_3^-	659 ± 34	11.53 ± 0.52	0.65 ± 0.02	4.87 ± 0.11
1a + $NOBF_4$	905 ± 28	7.06 ± 0.23	0.68 ± 0.01	4.34 ± 0.09
1a + $NOBF_4$ w/o TBP	866 ± 25	6.40 ± 0.43	0.59 ± 0.04	3.27 ± 0.12

To further prove the effect of TBP on the redox mediator based on **2a**, we made some devices with the same electrolyte but avoiding the presence of TBP. These devices showed V_{OC} values (ca. 600 mV) that agreed with the redox potential calculated by CV (Tab. 1) but also lower J_{SC} and FF leading to PCE slightly higher than 1%. Relying on these data, we can fairly assume that the sole solvent (at least at the concentration employed in the electrolytes) cannot replace a chelating ligand from the complex. As already discussed in the introduction, the couple **1a**/**1b** is a well-known standard as electrolyte in DSSCs. In this context, the partial oxidation of **1a** in **1b** was performed by means of $NOBF_4$ and the implementation of the so-obtained electrolyte in complete devices lead to more performing devices, as expected. The better photoelectrochemical parameters (PCE = 4.34%) are related to the more positive redox potential of **1a**/**1b** with respect to **2a**/**2b** leading to a higher V_{OC} and to less prominent recombination reactions.

Furthermore, ESI-MS analyses highlighted no evidence of ligand exchanges (Fig. S1). This was further confirmed by the similar photovoltaic behaviour of parent TBP-free devices whose lower PCE is mainly ascribable to a worse FF. As a further comparison, we made a device employing a standard iodide/triiodide redox couple. The latter experimented a higher J_{SC} (11.53 mA·cm^{-2}) and better PCE (4.87%) that could be ascribed to both an insufficiently fast diffusion of the Cu-based redox couple or to a lowering in the recombination reaction with I-based couple. In fact, it is worldwide accepted that metal-based redox couples seriously suffer for recombination reactions.

A further enhancement of photoelectrochemical properties could be expected following on from the amelioration of the morphological and electronic properties of the photoanode. This will be tackled in a forthcoming paper. Yet, the reported photoconversion efficiency is quite interesting especially considering the adoption of a semi-transparent photoanode.

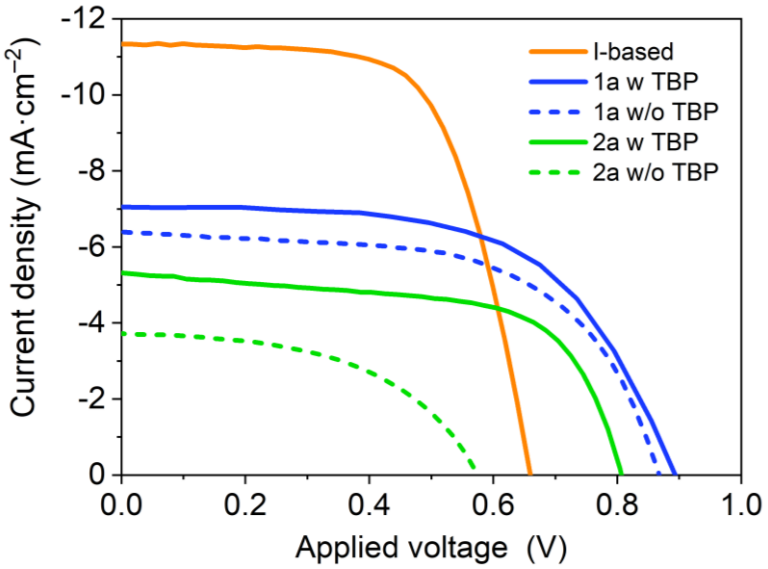

Fig. 5. . J-V curves of DSSCs using different electrolytes formulation: (i) iodine-based (orange). (ii) **1a**-based with (light blue) and without (dark blue) TBP and (iii) **2a**-based with (light green) and without (dark green) TBP.

4. Conclusions

Throughout the present paper we reported on the use of three different ligands employed to obtain six different homoleptic copper complexes (three couples of Cu(I) and Cu(II) systems). The optical and electrochemical properties of the latter were thoroughly investigated and the most promising ones have been implemented in semi-transparent Dye-sensitized Solar Cells. On one hand, compound **1a**, based on a simply modified bipyridine ligand, was selected as the literature benchmark, on the other **2a** was designed to clarify the role of a methoxy moiety (replacing the methyl of **1a**) in terms of both electronic and proximity effect. **3a**, bearing imidazo[1,5-*a*]pyridine ligands, was specifically designed to increase the steric hindrance of the ligand and, straightforwardly, to deep the redox potential and reduce the reorganization energy of the resulting complex. Very interestingly, the methoxy moiety was proved to take part to the coordination of copper cation and a lower redox potential was found. On the other hand, both **1a** and **2a** were proved to be quite unstable (at low concentration at least) in acetonitrile and TBP, probably due to the occurrence of partial ligand exchange; this issue seems to be solved when higher concentration is employed. Unfortunately, **3a** shows unexpectedly low redox potential value preventing his application in complete DSSCs. Conversely, both **1a** and **2a** were implemented in device along with their in-situ produced oxidized counterpart. In presence of *tert*-butylpyridine as co-adsorbent, the device embedding **2a** redox mediator leads to unexpectedly high open circuit voltages, probably due to ligand exchange. This effect will be detailly studied in a forthcoming paper. The same effect was not observed for **2a**-based devices. The most performing device showed a PCE > 4.3% when a semi-transparent photoanode was sensitized with MK-2 dye.

Acknowledgements

This project (in the person of MG, MB and GV) has received funding from the European Union's Horizon 2020 Research and Innovation Programme under grant agreement no. 826013 (IMPRESSIVE). The authors acknowledge Prof. Claudia Barolo for profitable discussion.

References

1 C. K. Prier, D. A. Rankic, D. W. C. MacMillan, *Chem. Rev.*, 2013, **113**, 5322-5363.
2 A. J. Esswein, D. G. Nocera, *Chem. Rev.*, 2007, **107**, 4022-4047.
3 Q. Zhao, C. Huanga, F. Li, *Chem. Soc. Rev.*, 2011, **40**, 2508-2524.
4 A. Singh, L. Spiccia, Coord. Chem. Rev. 2013, **257**, 2607-2622.
5 R. D. Costa, E. Ortí, H. J. Bolink, F. Monti, G. Accorsi, N. Armaroli, *Angew. Chem.*, 2012, **51**, 8178-8211.
6 C. Bizzarri, E. Spulinga, D. M. Knolla, D. Volzb, S. Bräseac, *Coord. Chem. Rev.*, 2018, **373**, 49-82.
7 A. Hagfeldt, G. Boschloo, L. Sun, L. Kloo, H. Pettersson, *Chem. Rev.*, 2010, **110**, 6595-6663.
8 M. Wang, C. Grätzel, S. M. Zakeeruddin, M. Grätzel, *Energy Environ. Sci.*, 2012, **5**, 9394-9405.
9 Y. Saygili, M. Stojanovic, N. Flores-Díaz, S. M. Zakeeruddin, N. Vlachopoulos, M. Grätzel, A. Hagfeldt, *Inorganics*, 2019, **7**, 30.
10 C. A. Bignozzi, R. Argazzi, R. Boaretto, E. Busatto, S. Carli, F. Ronconi, S. Caramori, *Coord. Chem. Rev.*, 2013, **257**, 1472-1492.
11 N. Mariotti, M. Bonomo, L. Fagiolari, N. Barbero, C. Gerbaldi, F. Bella, C. Barolo, *Green Chem*., 2020, **22**, 7168-7218.
12 C. E. Housecroft, E. C. Constable, *Chem. Soc. Rev.*, 2015, **44**, 8386-8398.
13 A. J. Nozik, J. Miller, *Chem. Rev.*, 2010, **110**, 6443-6445.
14 C. Dragonetti, M. Magni, A. Colombo, F. Fagnani, D. Roberto, F. Melchiorre, P. Biagini, S. Fantacci, *Dalton Trans.*, 2019, **48**, 9703-9711.
15 C. Dragonetti, M. Magni, A. Colombo, F. Melchiorre, P. Biagini, D. Roberto, *ACS Appl. Energy Mater.*, 2018, **1**, 751-756.
16 A. Colombo, C. Dragonetti, M. Magni, D. Roberto, F. Demartin, S. Caramori, C. A. Bignozzi, *ACS Appl. Mater. Interfaces*, 2014, **6**, 13945-13955.
17 Y. Saygili, M. Stojanovic, H.-S. Kim, J. Teuscher, R. Scopelliti, M. Freitag, S. M. Zakeeruddin, J. E. Moser, M. Grätzel, A. Hagfeldt, *J. Phys. Chem. C*, 2020, **124**, 7071-7081.
18 A. Colombo, C. Dragonetti, D. Roberto, F. Fagnani, *Molecules*, 2021, **26**, 194.
19 I. Benesperi, H. Michaels, M. Freitag, *J. Mater. Chem. C*, 2018, **6**, 11903-11942.
20 M. Freitag, Q. Daniel, M. Pazoki, K. Sveinbjörnsson, J. Zhang, L. Sun, A. Hagfeldt, G. Boschloo, *Energy Environ. Sci.*, 2015, **8**, 2634-2637.

21 Y. Cao, Y. Saygili, A. Ummadisingu, J. Teuscher, J. Luo, F. Pellet, F. Giordano, S. M. Zakeeruddin, J. E. Moser, M. Freitag, A. Hagfeldt, M. Grätzel, *Nat. Commun.*, 2017, **8**, 15390.
22 R. Ilmi, I. J. Al-busaidi, A. Haque, M. S. Khan, *J. Coord. Chem.*, 2018, **71**, 3045-3076.
23 Y. R. Liu, S. C. Yiu, C. L. Ho, W. Y. Wong, *Coord. Chem. Rev.,* 2018, **375,** 514-557.
24 K. D. Karlin, J. K. Yandell, *Inorg. Chem.*, 1984, **23**, 1184-1188.
25 D. B. Rorabacher, *Chem. Rev.*, 2004, 104, 651-698.
26 W. L. Hoffeditz, H. J. Katz, P. Deria, G. E. Cutsail, M. J. Pellin, O. K. Farha, T. J. Hupp, *J. Phys. Chem. C*, 2016, **120**, 3731-3740.
27 S. Hattori, Y. Wada, S. Yanagida, S. Fukuzumi, *J. Am. Chem. Soc.*, 2005, **127**, 9648-9654.
28 M. Freitag, F. Giordano, Y. Wang, M. Pazoki, Y. Hao, B. Zietz, G. Boschloo, *J. Phys. Chem. C*, 2016, **120**, 9595-9603.
29 E. Fresta, G. Volpi, C. Garino, C. Barolo, R. D. Costa, *Polyhedron*, 2018, **140**, 129-137.
30 M. D. Weber, C. Garino, G. Volpi, E. Casamassa, M. Milanesio, C. Barolo, R. D. Costa, *Dalton Trans.*, 2016, **45**, 8984-8993.
31 G. Albrecht, C. Geisa, J. M. Ruhl, R. Göttlich, D. Schlettwein, *Org. Electron.*, 2019, **65**, 321-326.
32 G. Albrecht, C. Rössiger, J. M. Herr, H. Locke, H. Yanagi, R. Göttlich, D. Schlettwein, *Phys. Status Solidi B*, 2020, **257**, 1900677.
33 M. Tiecco, L. Testaferri, M. Tignoli, D. Chianelli, M. Montanucci, *Synthesis*, 1984, 736-738.
34 L. Y. Liao, X. R. Kong, X. F. Duan, *J. Org. Chem.*, 2014, **79**, 777-782.
35 G. Volpi, C. Garino, E. Fresta, E. Casamassa, M. Giordano, C. Barolo, G. Viscardi, doi.org/10.1016/j.dyepig.2021.109455.
36 M. Magni, R. Giannuzzi, A. Colombo, M. P. Cipolla, C. Dragonetti, S. Caramori, M. Manca, *Inorg. Chem.*, 2016, **55**, 5245-5253.
37 J. Cong, D. Kinschel, Q. Daniel, M. Safdari, E. Gabrielsson, H. Chen, L. Kloo, *J. Mater. Chem. A*, 2016, **4**, 14550-14554.
38 S. Kitagawa, M. Munakata, A. Higashie, *Inorg. Chem.*, 1984, **84**, 79-84.
39 J. R. Vig, *J. Vac. Sci. Technol. A*, 1985, **3**, 1027-1034.
40 L. Vesce, R. Riccitelli, *Prog. Photovolt.*, 2012, **20**, 960-966.
41 M. K. Nazeeruddin, A. Kay, I. Rodicio, R. Humphry-Baker, E. Müller, P. Liska, M. Grätzel, *J. Am. Chem. Soc.*, 1993, **115**, 6382-6390.
42 M. Magni, A. Colombo, C. Dragonetti, P. Mussini, *Electrochim. Acta*, 2014, **141**, 324-330.
43 Y. Saygili, M. Söderberg, N. Pellet, F. Giordano, Y. Cao, A. B. Munoz-García, S. M. Zakeeruddin, N. Vlachopoulos, M. Pavone, G. Boschloo, L. Kavan, J.-E. Moser, M. Grätzel, A. Hagfeldt, M. Freitag, *J. Am. Chem. Soc.*, 2016, **138**, 15087-15096.
44 A. Klein, K. Butsch, J. Neudörfl, *Inorg. Chim. Acta*, 2010, **363**, 3282-3290.
45 G. Volpi, E. Priola, C. Garino, A. Daolio, R. Rabezzana, P. Benzi, A. Giordana, E. Diana, R: Gobetto, *Inorg. Chim. Acta*, 2020, **509**, 119662.
46 A. M. Blanco-Rodríguez, H. Kvapilová, J. Sýkora, M. Towrie, C. Nervi, G. Volpi, S. Záliš, A. Vlček, Jr., *J. Am. Chem. Soc.*, 2014, **136**, 5963-5973.
47 G. Volpi, R. Rabezzana, *New J. Chem.*, 2021, **45**, 5737-5743.
48 G. Volpi, C. Garino, E. Priola, C. Magistris, M. Chierotti, C. Barolo, *Dyes Pigm.*, 2019, **171**, 107713.
49 G. Volpi, C. Garino, L. Salassa, J. Fielder, K. I. Hardcastle, R. Gobetto, C. Nervi, *Chem. Eur. J.*, 2009, **15**, 6415-6427.
50 L. Salassa, C. Garino, A. Albertino, G. Volpi, C. Nervi, R. Gobetto, K. I. Hardcastle, *Organometallics*, 2008, **27**, 1427-1435.
51 L. Kavan, Y. Saygili, M. Freitag, S. M. Zakeeruddin, A. Hagfeldt, M. Grätzel, *Electrochim. Acta*, 2017, **227**, 194-202.
52 Y. Wang, T. W. Hamann, *Chem. Commun.*, 2018, **54**, 12361-12364.
53 K. Kannankutty, C.-C. Chen, V. S. Nguyen, Y.-C. Lin, H.-H. Chou, C.-Y. Yeh, T.-C. Wei, *ACS Appl. Mater. Interfaces*, 2020, **12**,